Society of Medical Education & Research

2026, Volume 6, Issue 1, Page No: 18-38
ISSN: 3108-4826

Journal of Medical Sciences and Interdisciplinary Research

Integrated Genotypic and Phenotypic Surveillance Reveals the Evolutionary Dynamics of SARS-CoV-2 Variants During the First Four Years of the COVID-19 Pandemic

Santiago Morales[1]*, Laura Rojas[2], Camila Vega[1], Diego Molina[3]

[1] Department of Virology and Genomic Surveillance, Faculty of Medicine, University of Buenos Aires, Buenos Aires, Argentina.
[2] Department of Phenotypic Evolution and Variant Dynamics, Faculty of Medicine, Pontifical Catholic University of Chile, Santiago, Chile.
[3] Department of COVID-19 Epidemiology and Integrated Surveillance, Faculty of Medicine, National University of La Plata, La Plata, Argentina.

***E-mail** ✉ santiago.morales@med.uba.ar

Abstract

Sustained phenotypic characterization and molecular epidemiological monitoring are crucial for the ongoing surveillance of newly emerging SARS-CoV-2 lineages. In this work, we implemented practical approaches to monitor the appearance, dissemination, and biological properties of SARS-CoV-2 variants across Australia at a time when diagnostic PCR testing had substantially declined, and research relied more heavily on targeted cohort studies. These activities were integrated with long-term investigations spanning four years of the COVID-19 pandemic. Throughout 2023, we collaborated with diagnostic pathology services and genomics laboratories to detect circulating and newly arising variants in the New South Wales (NSW) population. We evaluated these variants using viral isolation in culture, assessment of replication dynamics, neutralization assays, and evaluation of entry mechanisms dependent on ACE2 and TMPRSS2 receptors. To place these observations in the wider pandemic context, we performed ongoing longitudinal monitoring of neutralizing antibody activity at the population level using pooled intravenous immunoglobulins (IVIG) obtained from over 700,000 donations. Antibodies in both recent individual plasma samples and large IVIG pools derived from thousands of donations retained neutralizing capability against historical and contemporary SARS-CoV-2 variants. The variants EG.5.1, HV.1, XCT, and JN.1 displayed the strongest capacity to evade neutralization. Specific modifications at Spike positions 452, 455, and 456 in the type I antibody epitope region correlated with reduced neutralization titers in XBB lineages. Over three years of population-level immunity tracking, neutralization breadth against all tested SARS-CoV-2 variants continued to expand. Although early responses showed strong imprinting biased toward the Ancestral strain and pre-Omicron variants, this bias gradually diminished as cross-reactive neutralization broadened. We forecasted that JN.1 would confer a significant transmission benefit by late 2023, which was later confirmed by its worldwide predominance beginning in early 2024. This growth advantage was not primarily attributable to neutralization escape; rather, we suggest it resulted from enhanced utilization of ACE2 receptor populations that do not interact with TMPRSS2 via its Collectrin-Like Domain (CLD). Multiple SARS-CoV-2 lineages that arose toward the close of 2023 initially showed partial resistance to neutralization. Over time, this limitation was increasingly overcome by the progressive development of broader cross-reactive neutralizing responses. The eventual dominance of the highly divergent JN.1 lineage cannot be explained by neutralization resistance alone. Our results indicate that its success arose from the interplay between moderate immune evasion and altered preferences for ACE2/TMPRSS2-mediated cellular entry.

Keywords: SARS-CoV-2, Molecular epidemiology, ACE2, TMPRSS2, Collectrin-like domain, Neutralisation

Access this article online https://smerpub.com/

Received: 03 October 2025; **Accepted:** 15 January 2026

How to cite this article: Morales S, Rojas L, Vega C, Molina D. Integrated Genotypic and Phenotypic Surveillance Reveals the Evolutionary Dynamics of SARS-CoV-2 Variants during the First Four Years of the COVID-19 Pandemic. J Med Sci Interdiscip Res. 2026;6(1):18-38. https://doi.org/10.51847/obZsMhKtjB

Introduction

The coronavirus disease 2019 (COVID-19) pandemic has progressed to a stage in which community-level immunity is sustained by periodic, smaller-scale vaccine campaigns combined with recurrent infection waves. Although worldwide tracking of daily case counts and vaccine administration has markedly decreased, robust,

ongoing genomic and phenotypic surveillance of emerging SARS-CoV-2 variants remains critical. Such monitoring, consistent with surveillance practices for other viral epidemics, facilitates the prompt detection of changes in the virus's capacity to evade immune defenses or modify its cellular entry mechanisms [1], thereby informing timely public health interventions when necessary.

In the early phase of the pandemic, access to contemporary viral isolates was readily accomplished through diagnostic-research collaborations [1] that utilized residual PCR-positive clinical specimens for viral culture and full-genome sequencing. The widespread adoption of Rapid Antigen Tests (RATs) and the subsequent decline in diagnostic PCR testing significantly limited the availability of remnant samples suitable for swift phenotypic assessment. To address these constraints, we developed a genotype-to-phenotype surveillance network. Complementing routine genomic monitoring and molecular epidemiological analyses conducted in New South Wales, Australia (NSW), we incorporated national and international data on variant frequencies and competitive growth dynamics derived from the GISAID repository. This integration provided an efficient strategy for prioritizing candidate emerging variants for detailed investigation. Phenotypic evaluation was closely aligned with genomic surveillance through concurrent viral isolation and characterization pipelines, enabling rapid determination of neutralization profiles and cell-surface entry requirements for circulating strains. We then integrated these findings with longitudinal cohort studies that tracked neutralization responses and entry factor utilization for dominant variants across the first three years of the pandemic (2020 to late 2023). Incorporating these longitudinal neutralization datasets offered several key advantages. It allowed us to map immune response trajectories following major immunological milestones, such as vaccination campaigns and infection surges. It also supplied essential historical context for interpreting contemporary immune profiles. Finally, it enabled parallel examination of evolving viral entry preferences over the same timeframe. For the latter analyses, we generated stable clonal cell lines co-expressing ACE2 and TMPRSS2 in two distinct configurations. The first utilized wild-type (WT) ACE2 together with TMPRSS2, which effectively distinguishes pre-Omicron lineages (showing enhanced replication) from Omicron lineages (showing reduced replication). The second configuration replaced wild-type ACE2 with a well-characterized mutant form, designated C4 ACE2 [2, 3], in which the known TMPRSS2 interaction site at the Collectrin-like domain (CLD) in the neck region of ACE2 has been disrupted.

We propose that these two systems approximate physiologically relevant ACE2–TMPRSS2 arrangements. The wild-type configuration corresponds to ACE2 with an accessible Collectrin-Like Domain (CLD) available for TMPRSS2 engagement, consistent with proteolytic regulation of soluble ACE2 within the renin-angiotensin-aldosterone system (RAAS). The C4 mutant configuration reflects situations in which ACE2 functions as a chaperone for solute carrier proteins such as SLC6A19 and SLC6A20 [4, 5], whereby TMPRSS2 is sterically prevented from interacting with the CLD due to heterodimer formation. Thus, the C4 ACE2 mutant serves as a practical model for TMPRSS2 exclusion by eliminating its established binding site at the CLD.

In the present study, we report persistent neutralization resistance in recently circulating variants, including HK.3, XCT, and JN.1. However, longitudinal datasets demonstrate progressive maturation of host neutralizing responses over time that counteract these viral adaptations. In addition, we document ongoing viral evolution toward entry phenotypes that can be efficiently evaluated using the dual ACE2–TMPRSS2 clonal cell line platforms. Collectively, these observations reveal two dominant evolutionary trajectories across the first three years of the pandemic. First, although neutralizing immunity has developed more slowly than resistance in successive variants, it continues to exert selective pressure on emerging lineages. Second, while the entry characteristics of early SARS-CoV-2 resembled those of SARS-CoV-1—marked by enhanced replication in the presence of TMPRSS2 and ACE2—subsequent evolution has progressively shifted away from this route, with current variants strongly favoring ACE2 populations in which TMPRSS2 cannot engage the CLD.

Materials and Methods

Polyclonal immunoglobulin preparations and anti-SARS-CoV-2 hyperimmune globulin

Polyclonal IgG preparations were generated through the established, fully validated commercial manufacturing protocol utilized for Privigen [6]. Batches of Privigen were produced according to the standard Privigen procedure [6] and consisted of plasma obtained via

plasmapheresis from a mixed donor pool. This pool included individuals immunized with SARS-CoV-2 mRNA vaccines, those who had recovered from infection, and donors without recent infection history. Each batch incorporated roughly 15,000 donations collected in the United States spanning May 2020 to June 2023.

Human plasma

To augment the findings from IVIG evaluations, we analyzed plasma specimens collected in the first half of 2023 from cohorts with detailed records of vaccination and infection histories. The final ADAPT cohort—derived from an ongoing observational study that follows individuals after COVID-19 infection [7]—comprised recent 2023 donations from participants who had completed a primary vaccination series with boosters and experienced a documented BA.1 infection. This immunological background represents a substantial segment of the population in NSW's primary surveillance area.

The Australian Red Cross Lifeblood (Lifeblood) cohort (LIFE) included 44 plasma samples drawn from volunteers donating whole blood or plasma. All selected donors had been infected with SARS-CoV-2 and received vaccination, with each having completed at least two vaccine doses and reporting an infection episode between August 2022 and March 2023. Infection status was verified by rapid antigen testing.

Cell culture

HEK293T cells (Thermo Fisher Scientific, #R70007, RRID: CVCL_0063) stably expressing human ACE2 and TMPRSS2 were generated by lentiviral transduction following established protocols [1, 7]. Through clonal selection, we isolated a highly permissive clone designated HAT-24 and used it throughout this investigation. This HAT-24 line has been comprehensively cross-validated against the VeroE6 cell line [1]. VeroE6-TMPRSS2 (Vero-T) cells were kindly donated by Professor Alex Khromykh (University of Queensland). These represent the parental VeroE6 cell line (ATCC® CRL-1586™), modified by lentiviral delivery of the TMPRSS2 gene, as outlined in earlier work [8]. Both HAT-24 and Vero-T cells were propagated in Dulbecco's Modified Eagle Medium (Gibco, 11995073) supplemented with 10% fetal bovine serum (Gibco, 10099141; DMEM-10%FBS). All cultures were maintained at 37 °C in a humidified incubator with 5% CO_2 and relative humidity exceeding 90%. The Vero-T cells were authenticated according to previously published methods [8]. Subsequent modification of Vero-T cells involved lentiviral transduction to introduce either ACE2 or C4-ACE2 (RRID: CVCL_0574) as previously described [1], after which single-cell sorting was performed, and a single clonal derivative was selected for all downstream applications. Successful expression of human ACE2 was validated by flow cytometry, followed by genomic DNA extraction and sequencing of the human ACE2 locus or its C4-ACE2 variant. Short Tandem DNA Repeat (STR) profiling data for HAT-24 have been reported in a prior publication [1]. Primary bronchial epithelial cells (pBEC) were obtained from P. A. B. Wark (University of Newcastle) via bronchoscopy from donors who gave written informed consent. The experimental work was conducted with ethical approval from the University of Newcastle Safety Committee (Safety REF# 25/2016 and R5/2017). All donors underwent fibre-optic bronchoscopy in compliance with standard guidelines [9]. pBEC were expanded and allowed to differentiate until they formed a confluent monolayer in complete Bronchial Epithelial Cell Growth Basal Medium (Lonza, CC-3171) before being used for air–liquid interface (ALI) experiments. Unless otherwise stated, all cell cultures were incubated at 37 °C with 5% CO_2 and > 90% relative humidity. Regular testing confirmed the absence of mycoplasma contamination in all cell lines using the Lonza MycoAlert detection kit.

Virus isolation, expansion, and titration

All work with live SARS-CoV-2 was performed under biosafety level 3 (BSL-3) containment, following approved institutional safety procedures. SARS-CoV-2 variants were isolated and characterized following methods reported in earlier studies [1, 10]. Briefly, RT-qPCR-positive nasopharyngeal swabs from diagnostic specimens were passed through a sterile 0.22 μm filter by centrifugation at 10,000 g, then subjected to serial 1:3 dilutions before inoculation onto HAT-24 cells (5×10^3 cells per well in 384-well plates). Supernatants (300 μL; passage 1) collected from wells displaying clear cytopathic effects under light microscopy were transferred to 0.5×10^6 Vero-T cells cultured in 6-well plates with 2 mL MEM-2%FBS. These cultures were maintained under standard conditions (37 °C, 5% CO_2) until prominent cytopathic effects appeared, typically within 24–72 h. The harvested supernatant (passage 2)

was clarified by centrifugation at 3000 rpm for 10 min, stored at −80 °C, and later thawed to quantify the median 50% tissue culture infectious dose ($TCID_{50}$/mL) on Vero-T cells via the Spearman-Karber method [11]. Passage 3 virus stocks were produced by infecting Vero-T cells at an MOI of 0.025 for 24 h; supernatants were then collected, clarified, and frozen using the same procedure. The genomic sequence identity and integrity of passage 1 and passage 3 materials were confirmed by whole-genome sequencing on the Oxford Nanopore platform, as detailed previously [1, 12]. For titration of passage 3 stocks, serial 1:5 dilutions were prepared in DMEM-5%FBS and added to HAT-24 cells (1.6×10^4 cells/well in 384-well plates) that had been pre-stained with 5% v/v nuclear dye (Invitrogen, R37605). Following a 20 h incubation, total nuclear counts per well were measured with an IN Cell Analyzer 2500HS high-content imaging system and analyzed using IN Carta software (Cytiva, USA). Raw counts were normalized to generate sigmoidal dose–response curves (mock-infected wells defined as 100% and wells exposed to the highest virus concentration as 0%), from which median Virus Effective (VE_{50}) values were derived using GraphPad Prism software.

Abbott architect SARS-CoV-2 anti-Nucleocapsid IgG

Antibodies of the IgG class specific to the SARS-CoV-2 nucleocapsid (N) protein were quantified using the Architect SARS-CoV-2 IgG assay (Abbott Diagnostics, Sydney, NSW, Australia) according to methods reported earlier [7].

Flow cytometry cell-based assay for detection of SARS-CoV-2 antibodies

Patient sera were evaluated for reactivity against SARS-CoV-2 antigens via a flow cytometry platform as detailed in prior publications [7]. HEK293 cells were transiently transfected to express full-length Wuhan-1 Spike protein. Serum samples diluted 1:80 were incubated with the live transfected cells, followed by staining with AlexaFluor 647-labelled anti-human IgG (H+L) conjugate (Thermo Fisher Scientific). Acquisition was performed on an LSRII flow cytometer (BD Biosciences, USA).

Assay performance was validated against ten reference antibody preparations provided by the National Institute for Biological Standards and Control (NIBSC) under the CS678 protocol of the World Health Organization (WHO) international collaborative study for the first anti-SARS-CoV-2 antibody International Standard and Reference Panel. Analysis was undertaken using FlowJo 10.4.1 (TreeStar, USA), Microsoft Excel, and GraphPad Prism software.

R-20: rapid, high-content SARS-CoV-2 microneutralisation assay with HAT-24 cells

The R-20 microneutralization assay was performed on HAT-24 cells using a high-content imaging approach described previously [1, 7]. In short, plasma or IVIG samples were subjected to 1:2 serial dilutions in DMEM-5%FBS beginning at 1:10 (ancestral Clade A.2.2 samples initiated at 1:40). Virus stocks standardized to $2\times$ VE_{50} were mixed with the diluted sera or immunoglobulins and pre-incubated for 1 h at 37 °C with 5% CO_2. Forty microliters of each mixture (technical duplicates) were then added to 384-well plates containing nuclear-stained HAT-24 cells at 1.6×10^4 cells per well.

Following 20 h incubation, nuclear counts were determined with the IN Cell Analyzer 2500HS system. Percentage neutralization (%N) was calculated using the equation $\%N = (D - (1 - Q)) \times 100/D$, where [1] Q is the ratio of nuclei in test wells relative to uninfected controls (100% neutralization). D represents the corresponding value for virus-only controls (0% neutralization). IC_{50} titres (reciprocal dilution achieving 50% neutralization) were interpolated from sigmoidal curves generated in GraphPad Prism software.

Wild type ACE2/TMPRSS2 and C4-ACE2/TMPRSS2 entry assays using primary SARS-CoV-2

Stable cell lines co-expressing either wild-type (WT) ACE2 plus TMPRSS2 or the C4-ACE2 mutant plus TMPRSS2 were constructed following previously reported approaches [2].

Viral stocks were serially diluted (1:5) in MEM-2% FBS and added to cells plated in suspension at 5×10^3 cells per well in 384-well plates. After 72 h of incubation, cultures were stained with 5% v/v nuclear dye (Invitrogen, R37605). Total nuclear counts across each well were measured using an IN Cell Analyzer 2500HS high-content imaging platform and analyzed with IN Carta software (Cytiva, USA). Results were normalized to produce sigmoidal dose–response curves, with mock-infected controls set at 100% and the highest virus concentration set at 0%. Median Virus Effective (VE_{50}) values were calculated in GraphPad Prism software.

Modeling lineage dynamics

Evolutionary dynamics of viral lineages were examined through Bayesian multinomial logistic regression modeling of lineage abundance counts [13]. For the analyses presented in **Figures 1 and 2**, we retrieved the most current global SARS-CoV-2 sequence collection from GISAID [14] and restricted it to sequences sampled within the previous 100 days. Lineage classification used NextClade with the BA.2 reference ("sars-cov-2-21L"), accepting only sequences that met "good" quality control standards and had greater than 90% coverage. Daily counts were summed by country or region, limiting inclusion to locations with over 50 sequences in the most recent 50 days and more than 100 sequences in total. Low-frequency sub-lineages (fewer than 30 sequences) were consolidated under their most recent ancestral node based on the NextClade phylogeny.

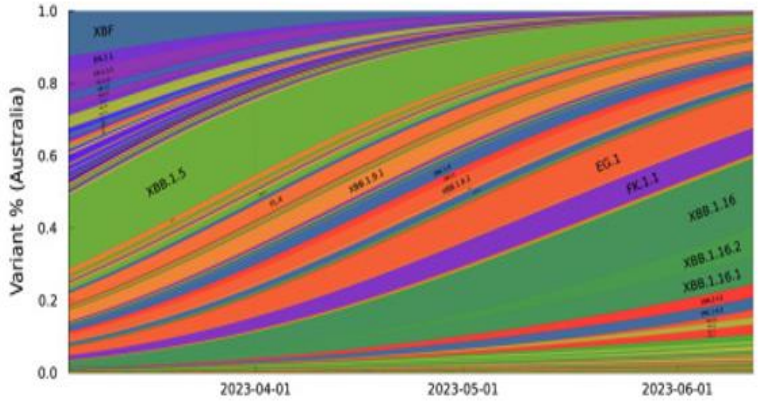

(a)

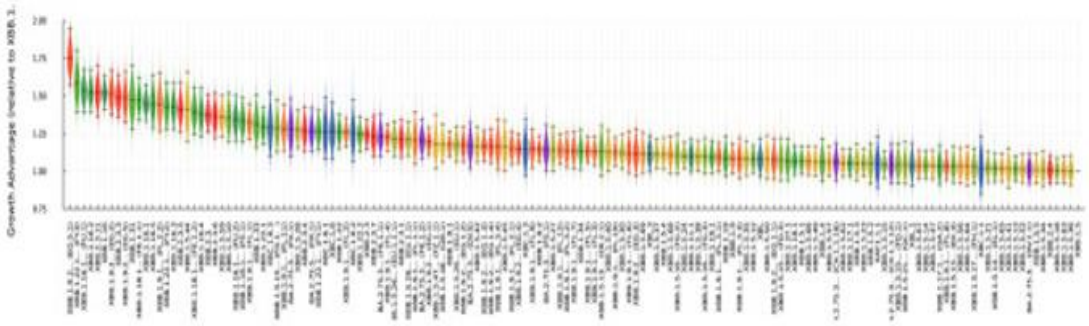

(b)

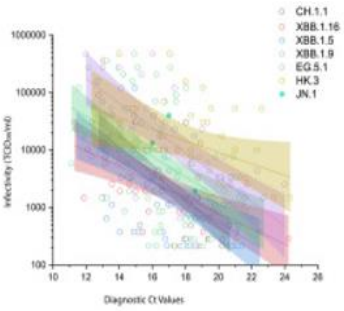

(c)

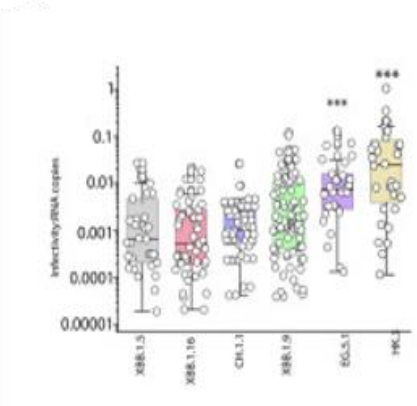

(d)

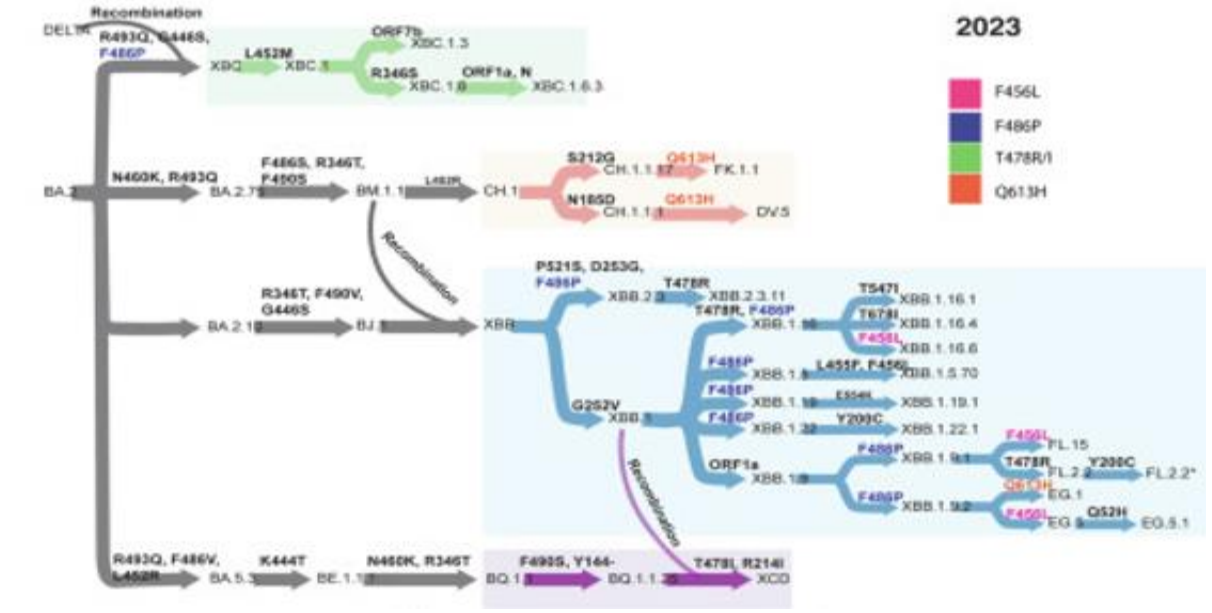

(e)

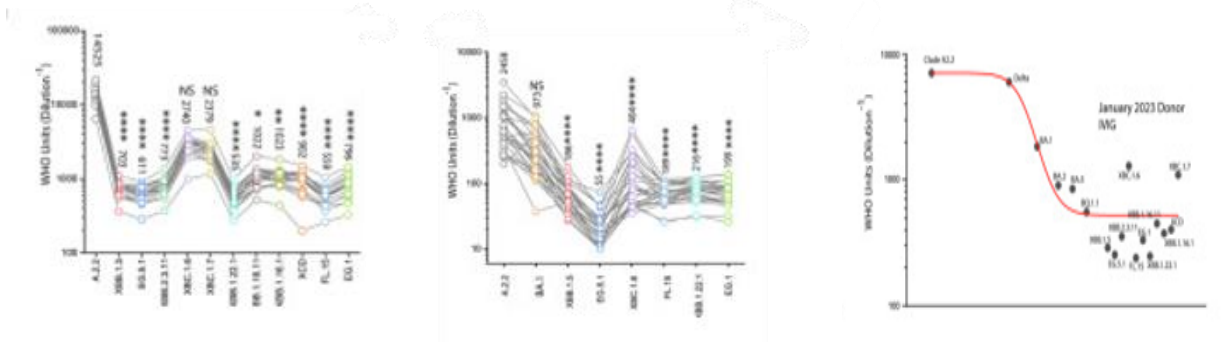

(f) (g) (h)

Figure 1. Consolidated model of SARS-CoV-2 surveillance in NSW, Australia and the appearance of convergent XBB lineages in mid-2023.

a) Genomic surveillance overview for Australia during June 2023 drawn from GISAID records. Each vertical band shows the posterior mean frequency projection derived from a hierarchical Bayesian multinomial logistic regression of variant competition. Two leading lineages are highlighted: XBB.1.16 (dark green) and XBB.1.9 (orange). b) Outcomes of global SARS-CoV-2 lineage competition modeling. Weekly multiplicative growth advantages are displayed for different lineages, benchmarked against both the parental BA.2 strain and the previously dominant XBB.1.5. c–d) Aggregate infectivity measurements from over 500 endpoint samples obtained from primary nasopharyngeal swabs throughout the 2023 diagnostic window. Lineages were clustered according to their closest parental origin (CH.1.1, XBB.1.5, XBB.1.9, XBB.1.16) or notable sub-lineages that acquired significant Spike alterations while maintaining substantial prevalence (such as EG.5.1 and HK.3 from XBB.1.9). Early JN.1 detections during this timeframe (n = 3) are shown for initial reference. c. Linear regression analysis relating viral infectivity ($TCID_{50}$/ml; y-axis) to diagnostic Ct values. Inferred RNA copies per diagnostic Ct value were employed to determine infectivity-to-RNA ratios, facilitating statistical evaluation between groups using the Mann–Whitney U test. e) By mid-June 2023, BA.2-descended Omicron lineages circulating in Australia had predominantly separated into several recombinant categories. From top to bottom: Delta-BA.2 recombinants of the XBC group, followed by non-recombinant CH.1.1 lineages; a broad XBB recombinant cluster including XBB.2.3, XBB.1.5, XBB.1.9,

XBB.1.19, XBB.1.22.1, and XCD; and BQ.1.1-derived lineages at the base. Shared Spike polymorphisms are color-coded: blue (F486P), pink (F456L), green (T478R/I), and orange (Q613H). f) Neutralization sensitivity of selected emerging variants identified between early and mid-2023, assessed against 20 IVIG batches derived from late 2022 U.S. donations. g) Neutralization sensitivity of the same variants tested using plasma from 2023 participants in the ADAPT cohort. h) Overview of neutralization trajectory using the latest 2023 IVIG batches. Dominant variants are arranged chronologically up to BQ.1.1, while other emerging strains appear independently of detection timing. The lowest neutralisation levels align with the top-ranked lineages in panel b, particularly EG.5.1 and XBB.1.22.1. Statistical comparisons in panels f and g of neutralising titres (WHO units/ml) relative to the Ancestral strain were conducted via Friedman's test followed by Dunn's multiple comparisons (* = $P < 0.05$; ** = $P < 0.01$; *** = $P < 0.001$; **** = $P < 0.0001$).

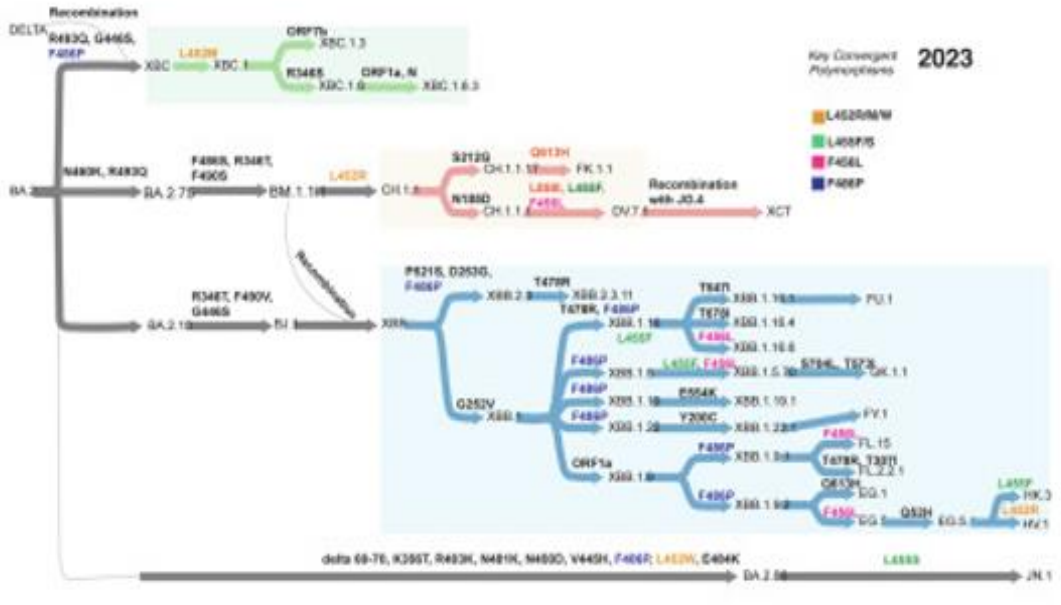

(a)

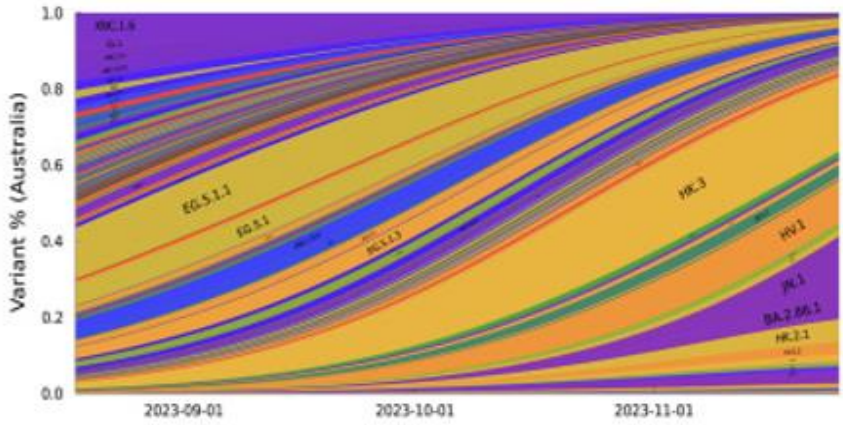

(b)

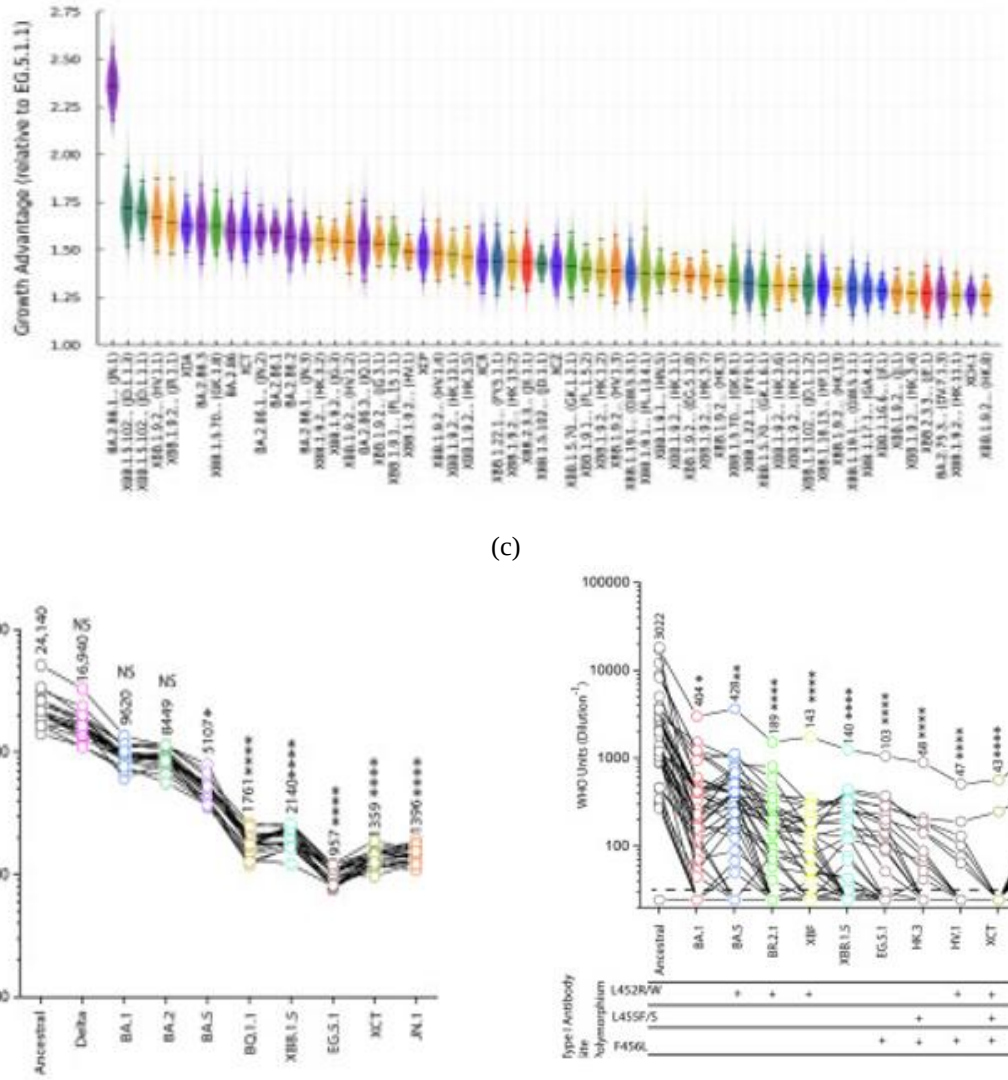

Figure 2. Neutralizing titers to emerging SARS-CoV-2 variants in late 2023.

a) Schematic representation of Omicron lineages descending from BA.2, depicting the distribution of emerging variants in Australia toward the end of 2023. Three primary clusters appear from top to bottom: Delta-BA.2 recombinants (XBC) together with CH.1.1 descendants that now encompass the recombinant XCT; XBB recombinants highlighted by the rise of HV.1 and HK.3 from EG.5.1; and the divergent BA.2.86 lineage with its sub-lineage JN.1 shown separately with defining mutations. Convergent Spike changes are indicated in blue (F486P), pink (F456L), green (L455F/S), and orange (L452R/M/W). b) Genomic surveillance snapshot for Australia in June 2023 based on GISAID. Vertical segments display posterior mean frequency estimates from the hierarchical Bayesian multinomial logistic model. Dominant lineages at this stage derived from EG.5.1 (HK.3 and HV.1; orange), with BA.2.86 and JN.1 (purple) appearing subsequently. c) Global lineage competition modeling results showing estimated weekly multiplicative growth advantages relative to both the parental BA.2 and the dominant EG.5.1 background. d–e) Live-virus neutralization titers measured using d. ten pooled IVIG samples manufactured from early-to-mid 2023 U.S. plasma donations (exact collection periods provided in supporting tables) and e. 44 individual Australian Lifeblood plasma donations collected chiefly during the latter half of 2023. IC_{50} values in panels d and e were determined for each tested variant and

benchmarked against ancestral Clade A.2.2 (= P < 0.001; = P < 0.0001). Statistical significance was evaluated by Friedman's test with Dunn's multiple comparisons. IC_{50} values were interpolated from four-parameter logistic sigmoidal regression curves fitted in GraphPad Prism version 9.1.2.

Modeling of growth rates

Growth rates were estimated through a hierarchical modeling framework. In this approach, the growth rate of each viral lineage in a particular geographic region equals the combination of an overall global rate and a random effect specific to that region. The global rate itself incorporates three distinct components: (i) terms linked to each ancestral branch preceding the lineage, (ii) coefficients for convergent spike mutations that arose independently on at least three separate occasions across the NextClade reference phylogeny and are found within the lineage, and (iii) a dedicated term unique to the lineage. This structure pools information from mutations shared across branches and accounts for phylogenetic heritability, meaning that growth rates of closely related lineages are expected, under the model prior, to be more similar. For recombinant lineages, growth terms are inherited as weighted averages drawn from multiple parental lineages.

Lineage-specific intercept parameters consist of one overarching shared term and additional random effects tailored to each region. Gaussian priors centered at zero were assigned to all parameter categories, supplemented by Gaussian hyperpriors on the logarithms of the associated standard deviations. Joint posterior sampling of global and local parameters across the complete global dataset was performed using Hamiltonian Monte Carlo with the No-U-Turn sampler, as implemented in the AdvancedHMC.jl package for Julia (https://proceedings.mlr.press/v118/xu20a.html).

Results shown in **Figure 1** (archived at: https://github.com/MurrellGroup/lineages/tree/be1851639b463876651e8cfceb5d075487d44651) derive from the global GISAID bulk download of 2023-06-12. Those in **Figure 2** (archived at: https://github.com/MurrellGroup/lineages/tree/93572151a4fae8dd10f00fa9d755b5cc69abd8de) are based on the 2023-11-25 bulk download. Current model estimates are publicly accessible at https://github.com/MurrellGroup/lineages.

Statistical methods

All statistical analyses were executed using GraphPad Prism 9 (GraphPad Software, USA). Linear correlations were assessed via regression fitting in OriginLab 9, with Pearson's r reported alongside ANOVA-derived P values to determine whether the regression slope was significantly different from zero. Sigmoidal dose-response relationships and corresponding IC50 values were calculated employing the four-parameter logistic (4 PL) sigmoidal regression model in GraphPad Prism. Datasets were first examined for normality to select appropriate downstream tests. Neutralization antibody titres against emerging variants were compared to those elicited by the ancestral A.2.2 strain using a two-tailed Friedman test followed by Dunn's multiple comparison procedure. The Mann–Whitney U test evaluated differences in infectivity-to-particle ratios among SARS-CoV-2 lineages in nasopharyngeal swab specimens and in infectious titres across engineered cell lines. Analyses involving primary cell cultures employed two-way ANOVA with Holm–Šídák post-hoc multiple comparisons. The respective figure legends provide comprehensive information on the statistical tests applied to individual datasets.

Ethical approval

This investigation received human research ethics clearance from the Lifeblood Research Ethics Committee under reference 30042020 and from St Vincent's Hospital for the ADAPT cohort under reference 2020/ETH00964. Blood donors signed consent forms explicitly authorizing the use of donations for research activities. NSW Health enabled access to de-identified residual diagnostic swabs from COVID-19 cases to assist the public health response, operating under the authority of Health Protection NSW.

Specimen collection procedures

Comprehensive PCR testing for COVID-19 during the pandemic offered exceptional opportunities for obtaining clinical material suitable for virus isolation. The subsequent widespread adoption of Rapid Antigen Tests and corresponding decline in PCR testing availability for the general public substantially limited access to samples required for detailed phenotypic studies. To maintain effective and timely surveillance of variant phenotypes, a collaborative network was formed among the NSW Ministry of Health, the NSW pathogen genomics reference laboratory, clinical diagnostic laboratories, and the Kirby Institute. Swab specimens originated primarily

from either a major diagnostic hub in Sydney serving 20 collection sites throughout the metropolitan area or from the Histopath diagnostic laboratory. The success of this diagnostic-research integration relied on upfront prioritization of samples displaying diagnostic cycle threshold (Ct) values below 25. A small aliquot (100 μL) of residual swab material was transferred into a coded container to ensure de-identification, promptly frozen at −80 °C within 24 hours, while the remainder underwent whole-genome sequencing. This workflow yielded viral isolation rates above 70% in the first half of 2023, with further improvements observed as new SARS-CoV-2 variant lineages appeared.

Funder involvement

The funding organizations played no role in study design, data collection, results analysis, or manuscript preparation. Investigators based at the Kirby Institute conducted all aspects of study design, data acquisition, analysis, and interpretation. Manuscript drafting and revision were performed exclusively by the research team.

Results and Discussion

Variant phenotypic surveillance conducted in australia, early 2023

In the initial six months of 2023, Australia's circulating SARS-CoV-2 variants were primarily composed of CH.1.1, XBB.1.16, and XBB.1.5. Later, those descending from XBB.1.9 (**Figure 1a**). Evaluation of competitive growth benefits across worldwide whole-genome sequencing data highlighted EG.5.1, a derivative of XBB.1.9, as exhibiting a clear selective advantage (**Figure 1b**).

Under the integrated phenotypic monitoring framework, primary virus isolation efficiency rose steadily during this period: 68% (n = 50) for CH.1.1 lineages, 72% (n = 51) for XBB.1.5 lineages, 74% (n = 36) for XBB.1.16 lineages, and 82% (n = 88) for XBB.1.9 lineages. As part of the phenotyping workflow, we determined the ratio of infectivity to viral load for individual nasopharyngeal swab specimens. This allowed us to assess whether infectivity, normalized to diagnostic Ct values, tracked the rise of successive variants. Swab infectivity per Ct value generally mirrored the modeled growth-advantage rankings. Although XBB.1.9 variants initially displayed a tendency for higher infectivity relative to Ct values, differences compared with concurrently circulating lineages remained modest (**Figures 1c and 1d**).

Subsequent emergence of the Spike substitutions F456L and L455F (**Figure 1e**) at the type I antibody epitope site in XBB.1.9-derived lineages EG.5.1 and HK.3 coincided with substantial enhancements in infectivity per diagnostic Ct value ($P \leq 0.005$, Mann–Whitney U test). These observations reinforced the variants' path toward predominance in the second half of 2023.

With access to several hundred primary isolates, we applied a structured prioritization protocol to focus detailed characterization on the most pertinent emerging strains. Prioritization integrated computed growth rates (**Figure 1b**) and rapid pooled-antibody screening to select high-priority samples from large cohorts for comprehensive testing. Twenty clinical-grade IVIG batches were utilized; each contained 10% IgG (w/v) pooled from roughly 15,000 donors across collection windows of approximately four weeks [15]. EG.5.1, FL.15, and XBB.1.22.1 proved among the most resistant to neutralization by these IVIG preparations (**Figure 1f**), consistent with their projected epidemiological expansion in mid-2023 (**Figure 1b**).

A curated selection of variants representing the spectrum examined against IVIG pools yielded neutralisation patterns at the individual level in the ADAPT cohort [7] that were largely concordant, except for EG.5.1, which produced the lowest titres overall (**Figure 1g**). Acknowledging the documented broadening of neutralising capacity in IVIG over successive periods [15], comparative evaluation focused on previously dominant strains versus those that rose to prominence in mid-2023 (**Figure 1h**). This analysis documented incremental declines in neutralisation titres from early Omicron BA.2 lineages through XBB.1.5 to the contemporary EG.5.1 and XBB.1.22.1 variants. Recombinant lineages stemming from the Delta–BA.2 hybrid XBC persisted in Australia across 2022–2023 and retained neutralization characteristics akin to Omicron BA.2 (**Figure 1h**).

Longitudinal assessment of population antibody responses to SARS-CoV-2 between 2021 and 2023 reveals principal immunological milestones of the pandemic thus far

We tracked anti-Spike IgG, anti-Nucleocapsid IgG, neutralizing antibody titers, and the breadth of neutralization over time and linked them to publicly available U.S. epidemiological proxies. These included

wastewater-based estimates of viral load (copies per mL, supplied by Biobot Analytics) as surrogates for case numbers, along with records of administered vaccine doses. By examining an aggregate of 688,199 plasma donations gathered from September 2021 to January 2023—commencing ahead of the peak third-dose vaccination campaign in the United States—the study captured developments from the waning of the Delta wave in late 2021 through January 2023 (**Figures 3a and 3b).** This window encompassed the majority of significant immunological occurrences, such as the third-dose booster campaign overlapping with the Omicron BA.1 wave (the most extensive infection surge in the U.S.), the BA.2 wave paired with a smaller booster effort, the BA.5 wave, the authorization and distribution of BA.4/5 bivalent vaccines, and the BQ.1 wave.

Increases in anti-Nucleocapsid IgG were evident soon after the Delta, BA.1, BA.5, and BQ.1 infection waves (**Figure 3a**). Although wastewater viral loads showed reduced magnitude during Omicron periods, they displayed comparable temporal trends across the three principal Omicron surges. Notably, anti-nucleocapsid IgG responses reached higher levels following the later BA.5 and BQ.1 waves, possibly due to immune recall triggered by frequent reinfections among a large segment of the population during these episodes (**Figure 3a**).

Neutralizing titers measured by live virus neutralization assay (LVNT) against the ancestral Clade A.2.2 peaked during the pandemic immediately after the widespread booster rollout (**Figure 3b**), coinciding with the largest recorded U.S. Omicron BA.1 infection wave. More modest LVNT elevations appeared with later booster programs, manifesting as smaller peaks during third- and fourth-dose administrations and the rollout of bivalent formulations (**Figure 3b**).

Further investigation of relationships among neutralization capacity, infection incidence, and vaccination involved plotting LVNT against anti-Nucleocapsid IgG (**Figures 3c–3e**) and LVNT against anti-Spike IgG (**Figures 3d–3f**). This analysis revealed no significant association between LVNT and anti-Nucleocapsid IgG (Pearson's r = 0.07796; P = 0.55039). Conversely, a clear positive correlation existed between LVNT and anti-Spike IgG (**Figure 3f)**; (Pearson's r = 0.4258; P < 0.0001). Taken together, the initial booster campaign and the extensive BA.1 infection wave produced substantial population immunity, with peak responses occurring at the start of 2022. The observed link between LVNT and anti-Spike IgG reflects cumulative Spike antigen exposure from both natural infection and vaccination and cannot differentiate between these sources. The pandemic peak thus corresponds to the convergence of multiple events that maximized Spike antigen exposure. In particular, the surge in vaccine doses overlapped with a major infection wave, as indicated by high wastewater viral loads during the spread of Omicron BA.1. This intense transmission phase fortunately occurred when many individuals had recently received their third vaccine dose, improving recognition of the divergent Omicron BA.1 variant [1]. After this wave subsided, subsequent LVNT increases were primarily driven by additional booster doses rather than new infection surges, resulting in stable titers around 10,000 WHO units/mL directed against ancestral Clade A.2.2.

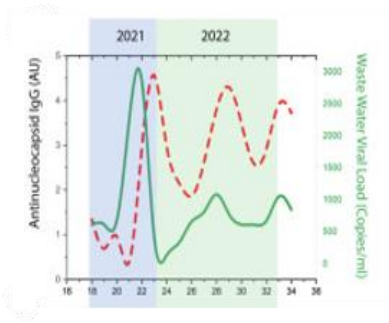

(a)

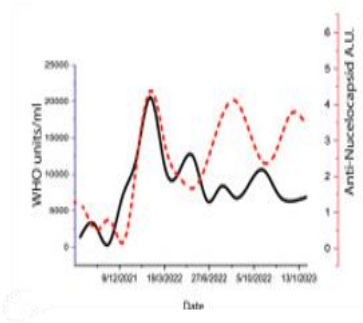

(c)

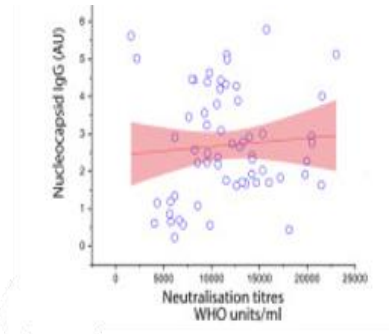

(e)

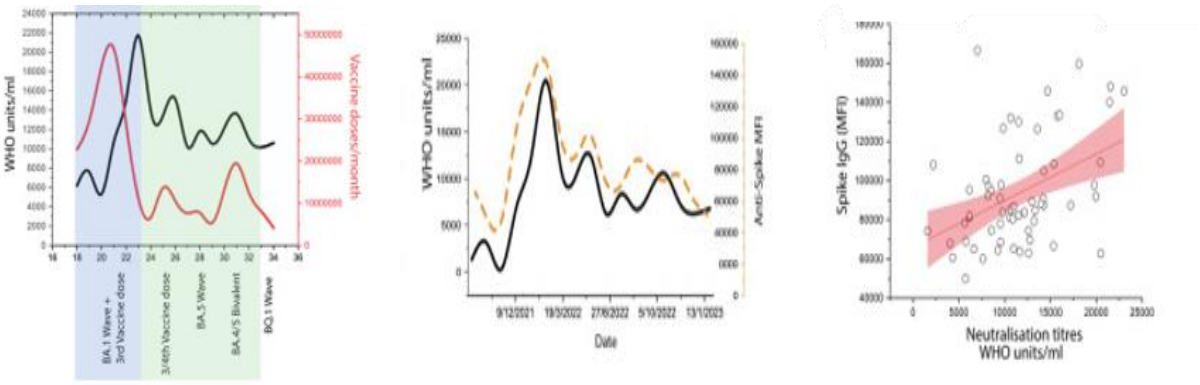

(b) (d) (f)

Figure 3. Pooled intravenous immunoglobulins (IVIGs).

a) Temporal profile of anti-Nucleocapsid IgG concentrations (dashed line) in pooled IVIG samples collected throughout the pandemic, starting after the Delta wave's decline and continuing until January 2023. The period captured multiple major immunological landmarks, including the Omicron BA.1 wave concurrent with peak third-dose vaccination, further third- and fourth-dose campaigns, the BA.5 wave, the BA.4/5 bivalent vaccine introduction, and the BQ.1 wave. Shading distinguishes 2021 events (blue) from those in 2022 (green). Cumulatively, the Privigen IVIG batches correspond to roughly 700,000 plasma donations. Time points reflect plasma collection dates for each batch, displayed as months elapsed since the pandemic's onset. The green line indicates average SARS-CoV-2 viral load in U.S. wastewater over the same timeframe (courtesy of Biobot Analytics: https://biobot.io/). b) Live virus neutralization titers (LVNT) of pooled IVIG against ancestral Clade A.2.2 (black line; endpoint titers normalized to WHO units/mL) plotted alongside COVID-19 vaccine doses administered (red line) during the corresponding interval (https://ourworldindata.org/). c) Comparison of LVNT (black line) with anti-Nucleocapsid IgG (red dashed line) in the Privigen batches from panel a. d) Comparison of LVNT (black line) with anti-Spike mean fluorescence intensity (MFI) levels (orange dashed line, assessed via flow cytometry) in the same batches. e–f) Correlations of LVNT (WHO units/mL) with e. anti-Nucleocapsid IgG and f. anti-Spike IgG. Pearson's r values were derived from linear regression performed in OriginLab. Associated ANOVA P values indicate whether the regression slope was significantly or non-significantly different from zero. Individual data points correspond to separate Privigen batches. MFI, mean fluorescence intensity.

Development of cross-reactive neutralizing breadth over the course of the COVID-19 pandemic surpasses original immunological imprinting

Extensive prior research has established that neutralizing antibody levels elicited through COVID-19 vaccination or infection decline markedly over time, enabling reinfection by newly arising variants [1, 16-18]. Parallel observations from our laboratory and independent groups indicate that this waning of titer intensity is offset by a gradual expansion in the range of variants recognized, signifying enhanced functional quality of the antibody response [15]. To characterize this population-wide broadening of neutralization over multiple years, we quantified LVNT against all prominent SARS-CoV-2 lineages that circulated during the preceding three years, using IVIG materials sourced between 2020 and 2023. Selection was limited to those variants that exceeded 50% prevalence among the relevant donor population in the United States (**Figure 4a**).

Titres were evaluated against Delta, Omicron BA.1, BA.2, BA.5, BQ.1.1, and XBB.1.5, using ancestral Clade A.2.2 as the benchmark. Appreciable neutralization persisted against the full set of Omicron sublineages examined, though generally at lower magnitudes than those observed for pre-Omicron strains (**Figures 4a and 4b**). A consistent pattern of rising titers to all variants emerged over successive periods, indicating accumulating cross-reactive capacity. Breadth was quantified as fold-change reductions in neutralization relative to the ancestral reference (**Figure 4c**). Across the entire timeframe, the highest titers remained directed

toward ancestral Clade A.2.2, unaffected even by the extensive Omicron BA.1 wave. This pattern is in keeping with high rates of prior vaccination and exposure to earlier circulating viruses, consistent with documented instances of original antigenic imprinting in multiple study populations [3, 19-24]. While initial imprinting effects were detectable, they were progressively mitigated as neutralization breadth extended to encompass antigenically distant variants.

Apart from Delta, which displayed near-equivalent neutralisation to the ancestral strain from the initial sampling points, the pace of breadth maturation proved comparable across all other variants examined (breadth linear slopes: BA.1 = 0.03159; BA.2 = 0.03264; BA.5 = 0.02449; BQ.1.1 = 0.03202; XBB.1.5 = 0.04002; overall mean slope 0.032 ± 0.0055). Such uniformity implies limited bias toward any particular post-infection or post-vaccination boosting event. Variant-specific differences were most evident in the baseline titre levels recorded in IVIG batches obtained immediately following the Delta wave (**Figure 4c**).

Projection of future breadth development relied on linear regression applied to temporal fold-reduction data (setting ancestral Clade A.2.2 to 1). Modeling began with early 2021 IVIG samples, the first to show detectable activity across the full variant panel. Extrapolating from fitted slopes, the estimated duration required for each Omicron lineage to attain neutralization parity with the ancestral strain ranged from approximately 0.33 years for BA.1 to around 2 years for XBB.1.5, using January 2023 as the reference starting point (**Figure 4c**). Slopes of breadth increase were essentially parallel for all Omicron variants (Delta excluded). Reanalysis using BA.1 rather than ancestral Clade A.2.2 as the comparator (**Figure 4d**) nearly eliminated positive slopes, reinforcing the parallel trajectories.

Given the consistency in expansion rates, the mean slope (0.032 ± 0.0055) was used to represent the overall rate of IVIG breadth maturation, capturing the positive trend observed across nearly two years of the pandemic. In addition to tracking breadth gains, the study assessed the concurrent rise in variant resistance to neutralization. Dominant lineages progressing from Delta to EG.5.1 were examined for increasing fold reductions in neutralization relative to ancestral Clade A.2.2 within individual IVIG batches, with linear regression applied to derive negative slopes. **Figure 4e** illustrates an example trajectory for the January 2023 batch. Across successive batches, the magnitude of these negative slopes diminished steadily (**Figure 4f**), indicating that newer IVIG preparations experienced slower titer losses as novel variants appeared. Assuming both breadth expansion and viral evasion rates remain stable, projections suggest that by June 2024 the rate of neutralization breadth improvement would equal and then outpace the rate of immune escape (**Figure 4f**).

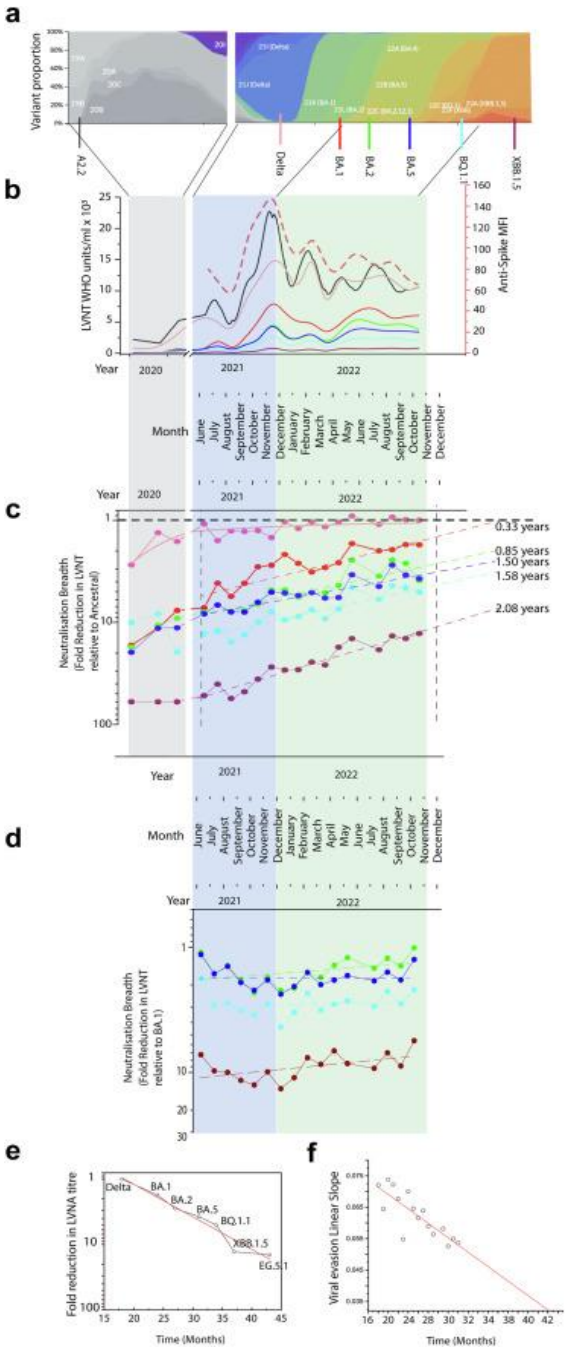

Figure 4. Expansion of neutralization breadth during the first three years of the COVID-19 pandemic.

a) Worldwide prevalence patterns of SARS-CoV-2 variants from early 2020 to mid-2023 (nextstrain.org). Major variants of concern attaining sustained prevalence above 50% within the U.S. donor population were chosen for evaluation, including ancestral Clade A.2.2, Delta, Omicron BA.1, BA.2, BA.5, BQ.1.1, and XBB.1.5. b) LVNT measured in pooled IVIG preparations, reported as WHO units/mL. The corresponding U.S. plasma donations totaled approximately 720,000 across the depicted interval. Coloured lines trace LVNT profiles for each variant shown in panel a. Dashed lines represent anti-Spike binding data from **Figure 3**, included for direct comparison with neutralization titers. c) Temporal changes in neutralization breadth for individual variants. Points indicate monthly average LVNT across all relevant IVIG batches, expressed as fold reduction versus ancestral (LVNT ancestral/LVNT variant). Early 2020 points for XBB.1.5 that fall below detection are capped at 60-fold. Dashed regression lines were fitted to data between late 2021 and early 2023 (vertical black dashed markers) and extended to forecast the period needed for breadth to converge on ancestral equivalence (fold reduction approaching 1). d) Breadth trajectories recalculated with Omicron BA.1 serving as the reference strain instead of ancestral Clade A.2.2. Resulting linear fits exhibit substantially flattened slopes relative to those in panel c. e) Example trajectory depicting progressive reduction in LVNT for one January 2023 IVIG batch (black line) as successive variants emerged chronologically. The computed negative slope of −0.0498 highlights ongoing loss of potency over time. f) Aggregate trajectories of variant evasion across multiple IVIG batches. White dots mark individual batches; more recent preparations display reduced negative slopes, reflecting slower titre declines against emerging variants as overall breadth improves. Assuming unchanging rates for both processes, breadth gains are projected to overtake viral evasion rates roughly 18 months after January 2023, corresponding to June 2024.

Rise of JN.1 during late 2023 and its supremacy over XBB.1 sublineages occur without major loss of neutralising activity

Throughout late 2023 in Australia, XBB-derived sublineages prevailed, marked by the progressive buildup of convergent substitutions at the type I antibody interaction region. Key changes involved L452R/M/W (orange), L455F/S (green), F456L (pink), and F486P (blue) (**Figures 2a and 2b**). Numerous XBB descendants harboring these shared mutations achieved high rankings in worldwide growth-advantage metrics. In particular, the recombinant XCT incorporated three type I antibody-site polymorphisms at Spike residues 452, 455, and 456. Meanwhile, prevalence remained limited for the newly emerged divergent lineage BA.2.86, first identified in Denmark and Israel [25]. Several BA.2.86 descendants ranked strongly in growth projections compared with XBB sublineages, most prominently the JN.1 sublineage carrying the defining L455S Spike substitution.

Following the methodology applied earlier in 2023, we prioritized the most current IVIG batches for evasion assessment, alongside individual-donor testing. Because population antibody breadth continues to mature, reliance on recently acquired donations was critical. Unlike the early 2023 situation, the sharp projected ascendancy of JN.1 together with convergent Spike alterations among XBB lineages (**Figures 2b and 2c**) allowed for more streamlined testing without extensive screening across expansive variant sets. Using the newest IVIG preparations (around June 2023), we evaluated a compact panel of variants representing both historically and currently dominant global strains. This selection comprised ancestral Clade A.2.2, Delta, Omicron BA.1, BA.2, BA.5, BQ.1.1, XBB.1.5, EG.5.1, XCT, and JN.1. EG.5.1 produced the weakest neutralization signals in this group, with XCT and JN.1 showing equivalently reduced yet closely comparable titres (**Figure 2d**).

In addition to population-representative IVIG testing, neutralization profiling was conducted using samples from individual donors in previously assembled cohorts. As many such cohorts had concluded, recent donations from the Lifeblood national plasma program served as a suitable source. The immunological backgrounds of these donors closely reflect experiences across Australian and global populations. Individual plasmas were challenged against 11 SARS-CoV-2 variants chosen according to their past and present circulation patterns in Australia. The panel included ancestral Clade A.2.2, Omicron BA.1, BA.5, BR.2.1, XBF, XBB.1.5, EG.5.1, HK.3, HV.1, XCT, and JN.1. Lowest titres were directed against XCT, with HV.1 only marginally higher. At the same time, HK.3 and JN.1 yielded median values akin to those for other widespread variants, including EG.5.1 and XBB.1.5 (**Figure 2e**). By comparison, considerably stronger LVNT persisted against ancestral and the dominant Omicron strains active in Australia during 2022 (BA.1, BA.5, BR.2.1, and XBF).

Overall, responses in pooled IVIG and individual donor samples exhibited notable alignment regarding SARS-CoV-2 variants. However, neutralization measurements alone failed to capture the pronounced projected growth advantage of JN.1 over other comparably evasive XBB descendants such as HK.3 and XCT.

Distinctive entry features of JN.1 relative to co-circulating sublineages involve favored utilization of TMPRSS2-Independent ACE2 at the collectrin-like domain

Sustained examination of entry mechanisms in evolving SARS-CoV-2 populations has traced a directional change in ACE2 reliance, progressing from initial ancestral Clade A viruses to modern Omicron forms [2] (preprint, not peer-reviewed). Given the additional dependence on TMPRSS2 for Spike subunit 2 (S2) cleavage, ACE2 engagement was investigated in environments featuring TMPRSS2 co-expression under dual configurations: one allowing TMPRSS2 interaction with the collectrin-like domain (CLD) of ACE2 and another disrupting this interaction site (**Figure 5a**) [2]. Co-expression of wild-type ACE2 with TMPRSS2 led to pronounced suppression of replication, exceeding attenuation levels seen in any earlier variant. Conversely, C4 CLD-mutated ACE2 supported modest replication enhancement (approximately 2-fold), though it did not reach statistical significance compared with prior lineages (**Figures 5c–5g**).

When plotted chronologically using representative primary isolates from ongoing phenotypic monitoring, utilisation of WT ACE2 in the presence of TMPRSS2 demonstrated a sustained reduction in infectivity over time (**Figure 5g**). JN.1 emerged as a notable exception, registering the lowest infectivity in this context (**Figure 5g**). Collectively, these patterns indicate that SARS-CoV-2 entry pathways have converged on ACE2 populations resistant to TMPRSS2 cleavage at the CLD, with no indication of return to the entry mode typical of the pandemic's earliest isolates. Validation in physiologically relevant primary cultures involved parallel expansion of XBB.1.5 and JN.1 followed by inoculation of air-liquid interface-differentiated upper airway epithelial cells at matched particle inputs. After three days, JN.1 generated significantly higher viral loads than XBB.1.5 ($P \leq 0.005$, two-way ANOVA with Holm–Šídák's multiple comparisons) (**Figure 5h**), confirming an entry adaptation conducive to superior competitive performance.

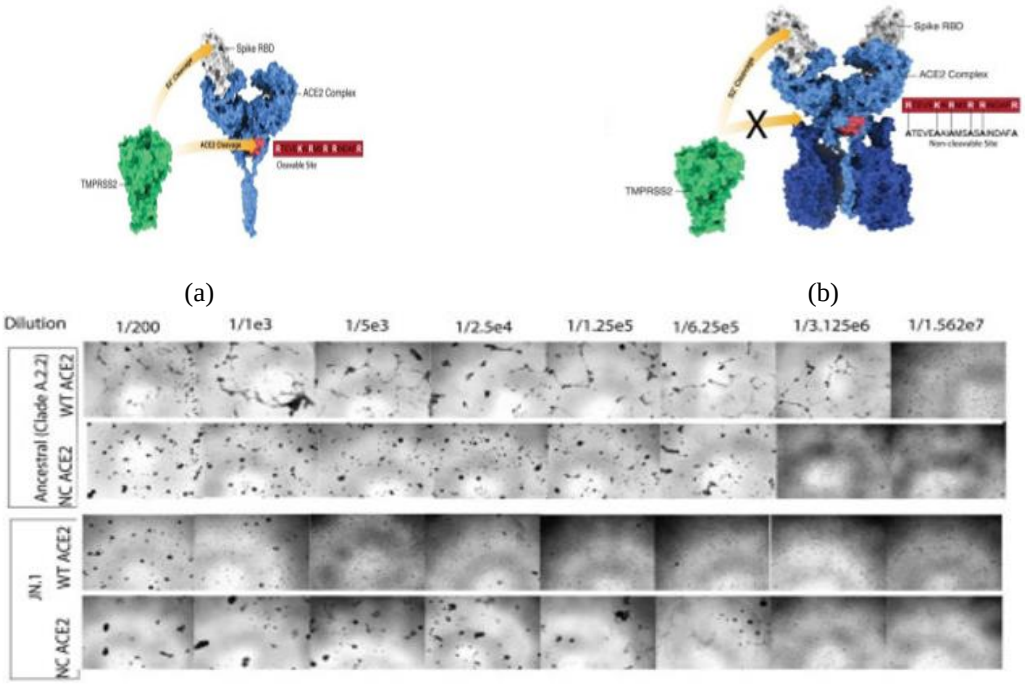

(a) (b)

(c)

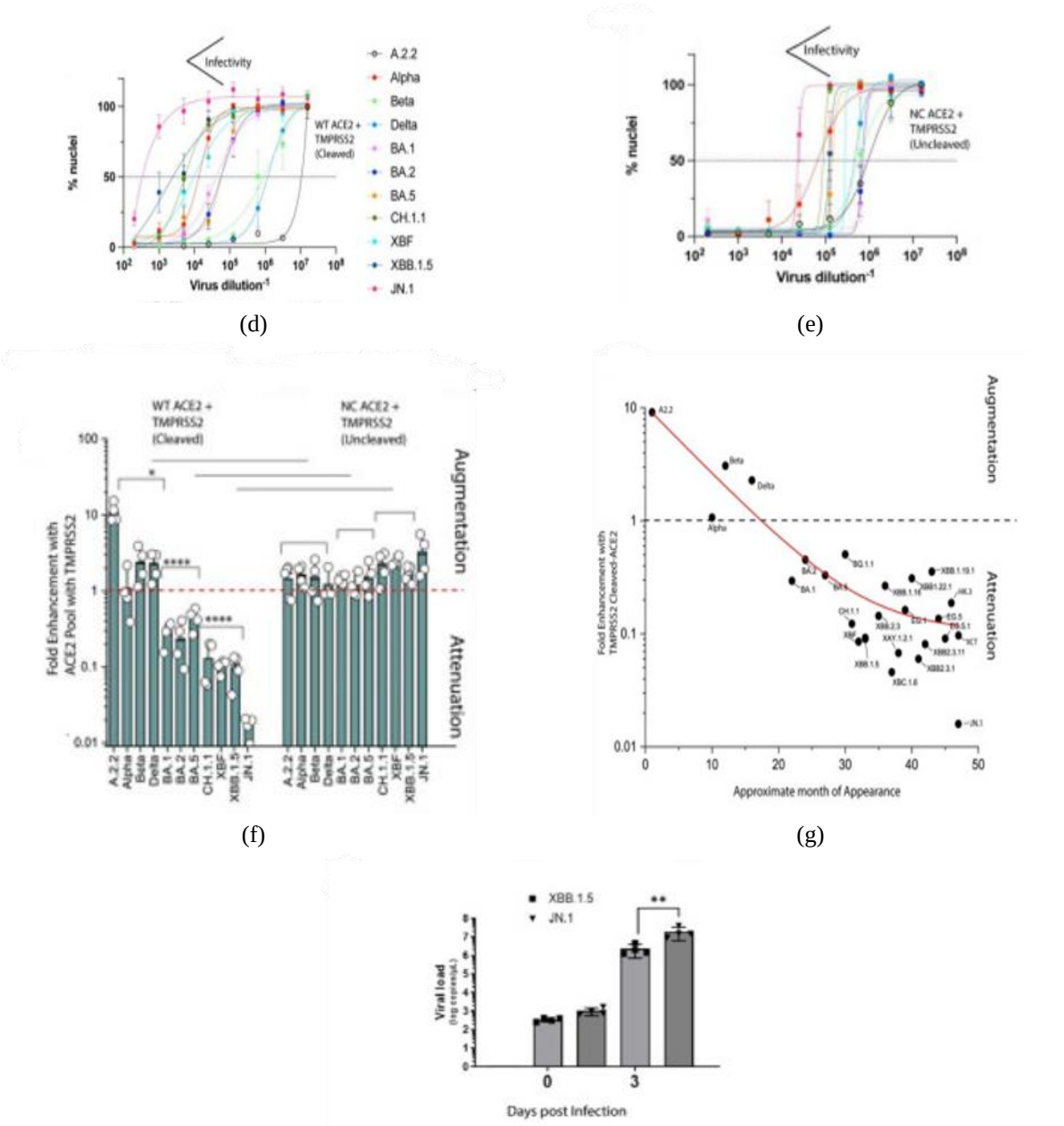

Figure 5. Progressive preference for TMPRSS2 cleavage-resistant ACE2 and superior replication of JN.1 compared with XBB.1.5 in primary upper respiratory tract epithelial models.

a) ACE2 dimer structure (blue) derived from the published model [26], indicating the TMPRSS2 cleavage site (pink) and recognition sequence (red box). Arrows denote TMPRSS2 cleavage positions on ACE2 and SARS-CoV-2 Spike (green). b) ACE2 dimer depicted as a heterodimer complex with solute carrier SLC6A19 (dark blue) per the published structure [26]. Associations with SLC6A20 or SLC6A19 near the TMPRSS2 site are predicted to block access. A TMPRSS2 cleavage-resistant ACE2 variant (NC-ACE2) was engineered as previously outlined [2]. c) WT ACE2 (cleavage-sensitive) and NC-ACE2 (cleavage-resistant) were co-expressed with TMPRSS2 in VeroE6 cells. Ancestral Clade A.2.2 and JN.1 were serially diluted, with cytopathic effects documented after two days. Upper panels: Clade A.2.2 dilutions; lower panels: JN.1 dilutions. d & e) Example dose-response curves in cells bearing d. wild-type ACE2 or e. cleavage-resistant ACE2

plus TMPRSS2. Replication was measured by loss of viable cell nuclei three days after infection (standard deviations from eight replicates). f) Summary of replication augmentation or attenuation for key pandemic variants (ancestral Clade A.2.2, Alpha, Beta, Delta, Omicron BA.1, BA.2, BA.5, XBB.1, CH.1.1, XBF, XBB.1.5, JN.1). Measurements performed in parental VeroE6-TMPRSS2 cells alongside WT ACE2 and NC-ACE2 lines from panel c. Red line denotes replication equivalent to the parental VeroE6-TMPRSS2 line. ∗ = P < 0.05 indicating reduced attenuation in NC-ACE2 vs WT ACE2; ∗∗∗∗ = P < 0.0005 for significant restoration in NC-ACE2 vs WT ACE2. g) Temporal profile of augmentation/attenuation for representative 2023 lineages as in panel f. Red line tracks declining dependence on cleavage-sensitive ACE2. h) Viral RNA loads in primary ALI cultures. XBB.1.5 and JN.1 clinical isolates were expanded and inoculated at equivalent RNA copies/mL. Supernatants were sampled for quantification. Values are mean ± s.d. from n = 3 experiments. ∗∗ = P < 0.005.

Within our ongoing SARS-CoV-2 monitoring program, spanning early 2020 to late 2023, we integrated cross-sectional assessments with longitudinal trends observed across the first four years of the COVID-19 pandemic. This integrated analysis included detailed characterization of humoral immune responses alongside elucidation of entry mechanisms utilized by primary viral isolates. Both lines of inquiry revealed progressive expansion of antibody breadth and an evolutionary convergence in viral entry factor utilization toward particular configurations of ACE2 and TMPRSS2. Collectively, these investigations draw upon primary clinical isolates and nearly one million plasma donations covering the first three years of the pandemic. Combined with contemporary cross-sectional evaluations of circulating variants, the findings delineate several critical "milestones" of the pandemic and highlight properties of current strains that suggest a favorable trajectory for antibody breadth maturation, alongside progressive refinement of viral entry pathways. These developments warrant more detailed in vivo investigation and closer correlation with clinical outcomes.

For the cross-sectional component conducted in 2023, expedited genotype-to-phenotype analyses indicated that neutralization against JN.1 was comparable to that observed for many late-circulating XBB sublineages. However, this similarity in neutralization sensitivity was insufficient to explain JN.1's observed growth superiority. In contrast, in vitro replication assays demonstrated that JN.1 has further refined its entry strategy, preferentially exploiting ACE2 populations incapable of supporting TMPRSS2 cleavage at the collectrin-like domain (CLD). This adaptation aligns with the broader evolutionary path documented throughout the pandemic. Accordingly, we propose that JN.1's competitive advantage arises from its capacity to effectively circumvent existing neutralizing antibodies while optimizing utilization of specific ACE2 subsets in conjunction with TMPRSS2.

At the population level, neutralizing responses appear to have stabilized following the peak of third-dose vaccinations and the concurrent extensive Omicron BA.1 wave. This stabilization persists despite declining booster uptake over time (https://ourworldindata.org/coronavirus) and community infection waves comparable in scale to recent Omicron BA.5 and BQ.1 surges. These temporal patterns at the population scale corroborate findings from numerous cohort studies and can be appreciated at multiple levels. First, the sustained robust responses against early variants are consistent with immunological imprinting induced by initial ancestral Clade-based vaccines and/or prior infection with early circulating strains such as Delta [19-24]. Second, detailed examination of responses to breakthrough infections and updated vaccine formulations has not identified clear lineage-specific targeting of distinct variant Spike glycoproteins [20, 27]. A prominent illustration is the dominant BA.1 wave, which, coinciding with widespread booster administration, generated the strongest neutralization directed against ancestral Clade and Delta viruses. Anti-Nucleocapsid responses also peaked during this period, underscoring the substantial contribution of BA.1 infections to overall population immunity. Likewise, the BA.5 wave drove additional elevations in anti-Nucleocapsid antibodies, yet this did not translate into specific broadening of LVNT against BA.5 sublineages. Although contributions from prior infections cannot be entirely excluded, the convergence of evidence from vaccine administration records, case incidence, wastewater viral loads, and comparative Spike versus Nucleocapsid antibody dynamics strongly implicates vaccination as the primary driver of increases in Spike-specific antibodies, LVNT, and initial imprinting toward ancestral clades. Reassuringly, the influence of early imprinting is gradually diminishing, as evidenced by comparable rates of breadth expansion across all variants over time. This uniform broadening is consistent with enhanced cross-reactivity at the individual donor level [27, 28]. Breadth approximately doubles over roughly one year (corresponding to halving the fold reduction in LVNT relative to ancestral), even as successive variants emerge to partially offset these gains.

This dynamic informed the cross-sectional surveillance conducted in late 2023, during which multiple divergent lineages such as HV.1, HK.3, and XCT accumulated convergent Spike polymorphisms capable of reducing LVNT. Nevertheless, XBB lineage dominance was supplanted by the emergence of JN.1, which exhibited substantially greater projected growth than co-circulating XBB derivatives despite comparable degrees of neutralization resistance [29-32].

At various points during the pandemic, surges driven by a single dominant variant frequently coincided with modifications in viral entry mechanisms in addition to reductions in LVNT. These adaptations included enhanced affinity for ACE2 [33] and more effective utilization of TMPRSS2, as documented for Delta and BA.5.1 [10]. Although progressive increases in ACE2 binding strength have been widely reported [33-40], the relationship between these changes and potential shifts in Omicron tropism from the lower to upper respiratory tract has not been clearly established. By generating cell lines with controlled variations in ACE2 and TMPRSS2 expression [2] (preprint, not peer-reviewed), we identified interactions between ACE2 and TMPRSS2 as an important contributor to evolving entry phenotypes, representing a third key parameter requiring thorough evaluation. Pre-Omicron lineages, along with SARS-CoV-1, exhibited substantial benefits from TMPRSS2 access to the CLD of ACE2 [3]. In contrast, early Omicron variants (BA.1 to BA.5) showed consistent attenuation under the same conditions. Likewise, CH.1.1, XBC, XBF, XBB.1.5, and especially JN.1 displayed progressively reduced infectivity when WT ACE2 was co-expressed with TMPRSS2 (with ancestral virus achieving approximately five orders of magnitude higher titres than JN.1 in this setting). Removal of TMPRSS2's capacity to engage the ACE2 CLD reversed this attenuation, with the degree of rescue becoming more pronounced in recent Omicron lineages, particularly JN.1.

Studies of JN.1 and its parental BA.2.86 lineage using primary clinical isolates in various cell systems have yielded inconsistent findings regarding tropism [30, 31, 41-44]. Pseudotype-based entry and fusion assays have also produced results that differ from those obtained with authentic JN.1 isolates [41, 43]. Nevertheless, the replication phenotype observed here aligns with other recent investigations employing primary JN.1 isolates in comparable cellular models [30]. Any surrogate measure of tropism should be correlated with clinical data or, where direct linkage is not feasible, with in vivo animal model observations. If the ACE2/TMPRSS2 interaction model accurately predicts lower respiratory tract behavior, early pre-Omicron isolates should replicate efficiently in lung tissue. In contrast, successive Omicron variants would show increasing attenuation. Supporting this notion, recent Syrian hamster studies comparing Omicron BA.5, EG.5.1, and JN.1 reported a gradient of attenuation ranked as BA.5 < EG.5.1 < JN.1 [45], consistent with independent work in the same model [42].

Physiological relevance of these ACE2–TMPRSS2 interactions is supported by the known tissue-specific roles of ACE2 in vivo. The CLD domain of ACE2 modulates shedding of soluble ACE2, a process integral to the renin-angiotensin-aldosterone system (RAAS) that is particularly active in the lower respiratory tract during acute injury [46]. In this compartment, the CLD is readily accessible to proteases such as TMPRSS2 and ADAM-17, favoring robust replication when ACE2 is available for TMPRSS2 engagement. Omicron lineages, however, are attenuated when ACE2 and TMPRSS2 interact freely, aligning with reduced replication potential in lung tissue. While these observations are consistent with a shift away from lower respiratory tropism, sustained transmission and dominance of lineages such as JN.1 would require efficient replication in alternative tissue sites.

In other tissues, ACE2 functions as a chaperone for solute carrier proteins such as SLC6A19 and SLC6A20, forming dimer-of-heterodimer complexes that position the solute carrier at residues (starting from ACE2 position 621), potentially shielding the TMPRSS2 cleavage site (beginning around residue 697) [5, 47]. Elevated expression of ACE2 and SLC6A19 in small intestinal enterocytes provides pools of ACE2 protected from TMPRSS2, offering a plausible environment for the evolution of variants such as JN.1. Although direct replication data for JN.1 in primary enterocytes are currently unavailable, increased fecal shedding observed in recent cohort studies supports enhanced replication at this site [48]. This does not fully account for superior growth in the upper respiratory tract. Notably, ACE2–SLC6A20 chaperone activity is also relevant to respiratory epithelium, and genetic studies have linked SLC6A20 polymorphisms to infection risk [49, 50]. These findings are consistent with our observations in primary air-liquid interface differentiated bronchial epithelial cells, where JN.1 demonstrates improved replicative capacity compared with XBB.1.5.

Given the persistence of SARS-CoV-2 and the recent refinement of JN.1 toward ACE2 pools decoupled from TMPRSS2, we hypothesize that a transmission benefit may derive from targeting ACE2 in its chaperone role with solute carriers rather than its RAAS-related functions. Future in vivo investigations will be essential

to clarify (1) how different ACE2 pools affect variant fitness and (2) whether such preferences influence tropism and associated clinical disease profiles.

We acknowledge that the present study is limited by its in vitro nature, and all findings require correlation with community transmission dynamics and clinical disease severity. The entry pathways delineated here demand deeper exploration through complementary in vitro and in vivo approaches, which are currently underway.

Conclusion

In conclusion, sustained cross-sectional and longitudinal monitoring of neutralizing responses to predominant SARS-CoV-2 variants remains crucial during this era of elevated case incidence and reduced vaccine uptake. Although breakthrough infections continue to elicit robust neutralization, the consequences of ongoing community and clinical infection waves require vigilant tracking. Parallel surveillance of viral entry requirements for historical and emerging lineages will be equally important for understanding impacts on disease severity within the prevailing immune landscape. Such knowledge will refine insights into viral tropism and the differential effects of acute versus chronic infection across tissues. Further research may indicate convergence toward the endemic pattern observed with longstanding seasonal human coronaviruses [51].

Nevertheless, continued vigilance is necessary. Pragmatic phenotypic surveillance of circulating community variants can rapidly inform adjustments to public health measures and vaccine strategies as required. Additionally, the extensive longitudinal datasets generated in this work provide a valuable resource for future pandemic preparedness, offering reference trajectories of population immunity and viral evolution during the acute phase of emerging threats.

Acknowledgments: None

Conflict of Interest: None

Financial Support: None

Ethics Statement: None

References

1. Aggarwal A, Stella AO, Walker G, Akerman A, Esler T, Milogiannakis V, et al. Platform for isolation and characterization of SARS-CoV-2 variants enables rapid characterization of Omicron in Australia. Nat Microbiol. 2022;7(6):896-8.
2. Anupriya A, Christina F, Vanessa M, Aggarwal A, Stella AO, Walker G, et al. TMPRSS2 activation of Omicron lineage Spike glycoprotein is regulated by Collectrin-like domain of ACE2. bioRxiv. 2023;2023.09.22.558930.
3. Heurich A, Hofmann-Winkler H, Gierer S, Liepold T, Jahn O, Pohlmann S. TMPRSS2 and ADAM17 cleave ACE2 differentially and only proteolysis by TMPRSS2 augments entry driven by the severe acute respiratory syndrome coronavirus spike protein. J Virol. 2014;88(2):1293-307.
4. Li HZ, Pike ACW, Lotsaris I, Gee CL, Yee SW, Kainosho M, et al. Structure and function of the SIT1 proline transporter in complex with the COVID-19 receptor ACE2. Nat Commun. 2024;15(1):5503.
5. Yan R, Zhang Y, Li Y, Xia L, Guo Y, Zhou Q. Structural basis for the recognition of SARS-CoV-2 by full-length human ACE2. Science. 2020;367(6485):1444-8.
6. Stucki M, Boschetti N, Schafer W, Hostettler T, Käsermann F, Nowak T, et al. Investigations of prion and virus safety of a new liquid IVIG product. Biologicals. 2008;36(4):239-47.
7. Tea F, Ospina Stella A, Aggarwal A, Darley DR, Pilli D, Vitale D, et al. SARS-CoV-2 neutralizing antibodies: longevity, breadth, and evasion by emerging viral variants. PLoS Med. 2021;18(7):e1003656.
8. Amarilla AA, Sng JDJ, Parry R, Modhiran N, Setoh YX, Liu X, et al. A versatile reverse genetics platform for SARS-CoV-2 and other positive-strand RNA viruses. Nat Commun. 2021;12(1):3431.
9. Workshop summary and guidelines: investigative use of bronchoscopy, lavage, and bronchial biopsies in asthma and other airway diseases. J Allergy Clin Immunol. 1991;88(5):808-14.
10. Aggarwal A, Akerman A, Milogiannakis V, Walker G, Stella AO, Kindinger F, et al. SARS-CoV-2 Omicron BA.5: evolving tropism and evasion of potent humoral responses and resistance to clinical immunotherapeutics relative to viral variants of concern. EBioMedicine. 2022;84:104270.
11. Ramakrishnan MA. Determination of 50% endpoint titer using a simple formula. World J Virol. 2016;5(2):85-6.
12. Bull RA, Adikari TN, Ferguson JM, Hammond JM, Stevanovski I, Beukers AG, et al. Analytical validity

of nanopore sequencing for rapid SARS-CoV-2 genome analysis. Nat Commun. 2020;11(1):6272.
13. Sheward DJ, Kim C, Fischbach J, Muschiol S, Ehling RA, Björkström NK, et al. Omicron sublineage BA.2.75.2 exhibits extensive escape from neutralising antibodies. Lancet Infect Dis. 2022;22(11):1538-40.
14. Shu Y, McCauley J. GISAID: global initiative on sharing all influenza data - from vision to reality. Euro Surveill. 2017;22(13).
15. Akerman A, Milogiannakis V, Jean T, Esler T, Aggarwal A, Walker G, et al. Emergence and antibody evasion of BQ, BA.2.75 and SARS-CoV-2 recombinant sub-lineages in the face of maturing antibody breadth at the population level. EBioMedicine. 2023;90:104545.
16. Willett BJ, Grove J, MacLean OA, Wilkie C, De Lorenzo G, Furnon W, et al. Publisher Correction: SARS-CoV-2 Omicron is an immune escape variant with an altered cell entry pathway. Nat Microbiol. 2022;7(10):1709.
17. Goldberg Y, Mandel M, Bar-On YM, Bodenheimer O, Freedman L, Haas EJ, et al. Protection and waning of natural and hybrid immunity to SARS-CoV-2. N Engl J Med. 2022;386(23):2201-12.
18. Tartof SY, Slezak JM, Fischer H, Hong V, Ackerson BK, Ranasinghe ON, et al. Effectiveness of mRNA BNT162b2 COVID-19 vaccine up to 6 months in a large integrated health system in the USA: a retrospective cohort study. Lancet. 2021;398(10309):1407-16.
19. Johnston TS, Li SH, Painter MM, Zarnitsyna VI, Li M, D'Souza C, et al. Immunological imprinting shapes the specificity of human antibody responses against SARS-CoV-2 variants. Immunity. 2024;57(4):912-25.e4.
20. Tortorici MA, Addetia A, Seo AJ, Brown J, Sprouse K, Logue J, et al. Persistent immune imprinting occurs after vaccination with the COVID-19 XBB.1.5 mRNA booster in humans. Immunity. 2024;57(4):904-11.e4.
21. Wang Q, Guo Y, Tam AR, Valdez R, Gordon A, Liu L, et al. Deep immunological imprinting due to the ancestral spike in the current bivalent COVID-19 vaccine. Cell Rep Med. 2023;4(11):101258.
22. Chemaitelly H, Ayoub HH, Tang P, Coyle P, Yassine HM, Al-Khatib HA, et al. Immune imprinting and protection against Repeat reinfection with SARS-CoV-2. N Engl J Med. 2022;387(18):1716-8.
23. Roltgen K, Nielsen SCA, Silva O, Younes SF, Zaslavsky M, Costales C, et al. Immune imprinting, breadth of variant recognition, and germinal center response in human SARS-CoV-2 infection and vaccination. Cell. 2022;185(6):1025-40.e14.
24. Aydillo T, Rombauts A, Stadlbauer D, Aslam S, Abelenda-Alonso G, Escalera A, et al. Immunological imprinting of the antibody response in COVID-19 patients. Nat Commun. 2021;12(1):3781.
25. Rasmussen M, Moller FT, Gunalan V, Baig S, Bennedbæk M, Christiansen LE, et al. First cases of SARS-CoV-2 BA.2.86 in Denmark, 2023. Euro Surveill. 2023;28(36).
26. Lan J, Ge J, Yu J, Shan S, Zhou H, Fan S, et al. Structure of the SARS-CoV-2 spike receptor-binding domain bound to the ACE2 receptor. Nature. 2020;581(7807):215-20.
27. Carreno JM, Singh G, Simon V, Krammer F; PVI study group. Bivalent COVID-19 booster vaccines and the absence of BA.5-specific antibodies. Lancet Microbe. 2023;4(8):e569.
28. Wang Q, Bowen A, Valdez R, Gherasim C, Gordon A, Liu L, et al. Antibody response to omicron BA.4-BA.5 bivalent booster. N Engl J Med. 2023;388(6):567-9.
29. Wang Q, Guo Y, Bowen A, Mellis IA, Valdez R, Gherasim C, et al. XBB.1.5 monovalent mRNA vaccine booster elicits robust neutralizing antibodies against XBB subvariants and JN.1. Cell Host Microbe. 2024;32(3):315-21.e3.
30. Planas D, Staropoli I, Michel V, Lemoine F, Donati F, Prot M, et al. Distinct evolution of SARS-CoV-2 Omicron XBB and BA.2.86/JN.1 lineages combining increased fitness and antibody evasion. Nat Commun. 2024;15(1):2254.
31. Kaku Y, Okumura K, Padilla-Blanco M, Kosugi Y, Uriu K, Hinay AA, et al. Virological characteristics of the SARS-CoV-2 JN.1 variant. Lancet Infect Dis. 2024;24(2):e82.
32. Jeworowski LM, Muhlemann B, Walper F, Schmidt ML, Jansen J, Krumbholz A, et al. Humoral immune escape by current SARS-CoV-2 variants BA.2.86 and JN.1, December 2023. Euro Surveill. 2024;29(2).
33. Yue C, Song W, Wang L, Jian F, Chen X, Gao F, et al. ACE2 binding and antibody evasion in enhanced

transmissibility of XBB.1.5. Lancet Infect Dis. 2023;23(3):278-80.
34. Li L, Liao H, Meng Y, Li W, Han P, Qiu T, et al. Structural basis of human ACE2 higher binding affinity to currently circulating Omicron SARS-CoV-2 sub-variants BA.2 and BA.1.1. Cell. 2022;185(16):2952-60.e10.
35. Barton MI, MacGowan SA, Kutuzov MA, Dushek O, Barton GJ, van der Merwe PA. Effects of common mutations in the SARS-CoV-2 Spike RBD and its ligand, the human ACE2 receptor on binding affinity and kinetics. Elife. 2021;10.
36. Ramanathan M, Ferguson ID, Miao W, Khavari PA. SARS-CoV-2 B.1.1.7 and B.1.351 spike variants bind human ACE2 with increased affinity. Lancet Infect Dis. 2021;21(8):1070.
37. Saito A, Tamura T, Zahradnik J, Deguchi S, Tabata K, Shishido T, et al. Virological characteristics of the SARS-CoV-2 Omicron BA.2.75 variant. Cell Host Microbe. 2022;30(11):1540-55.e15.
38. Kimura I, Yamasoba D, Tamura T, Nao N, Suzuki T, Oda Y, et al. Virological characteristics of the SARS-CoV-2 Omicron BA.2 subvariants, including BA.4 and BA.5. Cell. 2022;185(21):3992-4007.e16.
39. Zahradnik J, Marciano S, Shemesh M, Zoler E, Harari D, Chiaravalli J, et al. SARS-CoV-2 variant prediction and antiviral drug design are enabled by RBD in vitro evolution. Nat Microbiol. 2021;6(9):1188-98.
40. Motozono C, Toyoda M, Zahradnik J, Saito A, Nasser H, Tan TS, et al. SARS-CoV-2 spike L452R variant evades cellular immunity and increases infectivity. Cell Host Microbe. 2021;29(7):1124-36.e11.
41. Zhang L, Kempf A, Nehlmeier I, Cossmann A, Richter A, Bade N, et al. SARS-CoV-2 BA.2.86 enters lung cells and evades neutralizing antibodies with high efficiency. Cell. 2024;187(3):596-608.e17.
42. Tamura T, Mizuma K, Nasser H, Deguchi S, Padilla-Blanco M, Oda Y, et al. Virological characteristics of the SARS-CoV-2 BA.2.86 variant. Cell Host Microbe. 2024;32(2):170-80.e12.
43. Qu P, Xu K, Faraone JN, Goodarzi N, Zheng YM, Carlin C, et al. Immune evasion, infectivity, and fusogenicity of SARS-CoV-2 BA.2.86 and FLip variants. Cell. 2024;187(3):585-95.e6.
44. Khan K, Lustig G, Römer C, Reedoy K, Jule Z, Karim F, et al. Evolution and neutralization escape of the SARS-CoV-2 BA.2.86 subvariant. Nat Commun. 2023;14(1):8078.
45. Abdelnabi R, Lassauniere R, Maes P, Weynand B, Neyts J. Comparing the infectivity of recent SARS-CoV-2 omicron sub-variants in Syrian hamsters. Viruses. 2024;16(1).
46. Imai Y, Kuba K, Rao S, Huan Y, Guo F, Guan B, et al. Angiotensin-converting enzyme 2 protects from severe acute lung failure. Nature. 2005;436(7047):112-6.
47. Shen Y, Wang J, Li Y, Zhang Y, Tian R, Yan R. Structures of ACE2-SIT1 recognized by Omicron variants of SARS-CoV-2. Cell Discov. 2022;8(1):123.
48. Wannigama DL, Amarasiri M, Phattharapornjaroen P, Hongsing P, Hurst C, Badavath VN, et al. Increased faecal shedding in SARS-CoV-2 variants BA.2.86 and JN.1. Lancet Infect Dis. 2024;24(6):e348-50.
49. Roberts GHL, Partha R, Rhead B, Knight SC, Park DS, Coignet MV, et al. Expanded COVID-19 phenotype definitions reveal distinct patterns of genetic association and protective effects. Nat Genet. 2022;54(4):374-81.
50. Horowitz JE, Kosmicki JA, Damask A, Sharma D, Roberts GHL, Justice AE, et al. Genome-wide analysis provides genetic evidence that ACE2 influences COVID-19 risk and yields risk scores associated with severe disease. Nat Genet. 2022;54(4):382-92.
51. Cohen J. Covid's cold cousins. Science. 2024;383(6679):141-5.